

A Generalized Placeability Metric for Model-Free Unified Pick-and-Place Reasoning

Benno Wingender*

Nils Dengler*

Rohit Menon

Sicong Pan

Maren Bennewitz

Abstract—To reliably pick and place unknown objects under real-world sensing noise remains a challenging task, as existing methods rely on strong object priors (e.g., CAD models), or planar-support assumptions, limiting generalization and unified reasoning between grasping and placing. In this work, we introduce a generalized placeability metric that evaluates placement poses directly from noisy point clouds, without any shape priors. The metric jointly scores stability, graspability, and clearance. From raw geometry, we extract the support surfaces of the object to generate diverse candidates for multi-orientation placement and sample contacts that satisfy collision and stability constraints. By conditioning grasp scores on each candidate placement, our proposed method enables model-free unified pick-and-place reasoning and selects grasp-place pairs that lead to stable, collision-free placements. On unseen real objects and non-planar object supports, our metric delivers CAD-comparable accuracy in predicting stability loss and generally produces more physically plausible placements than learning-based predictors.

I. INTRODUCTION

The ability to pick objects and place them at desired locations is central to many robotics applications, including warehouse logistics, household assistance, and healthcare [1], [2]. Executing a pick and place task requires perceiving an object’s shape and pose, planning a stable grasp, determining how to place it securely and stable in the target region, and carrying out these steps reliably in clutter and under uncertainty. Rather than treating grasping and placing as separate problems, recent work performs joint reasoning over both stages [3], [4], [5], which we refer to as *unified pick-and-place reasoning*. By accounting for the target placement area during grasp selection, robots can choose grasps that both retrieve and place objects successfully, while avoiding collisions early and reducing re-grasping caused by environmental constraints.

However, most approaches [6], [7] assess the stability of candidate placements using strong object priors (e.g., CAD models), while others evaluate only a small, predefined subset of placement poses per grasp and rely on grasp-centric, hand-crafted objectives [3], [4], [8]. This can narrow down the search, induce local minima, and limit robustness under real-world noise. In contrast, a recent learning-based stable-plane predictor [9] can process unseen partial point clouds, but assumes planar supports and omits edge-proximal cases limiting generalizability. Consequently, the field still

All authors are with the Humanoid Robots Lab, University of Bonn, Germany. M. Bennewitz, M. Menon, S. Pan, and N. Dengler, are additionally with the Lamarr Institute for Machine Learning and Artificial Intelligence and the Center for Robotics, Bonn, Germany. This work has partly been supported by the BMBF within the Robotics Institute Germany, grant No. 16ME099.



Fig. 1: From a noisy object point cloud, our system evaluates candidate placements using the proposed generalized placeability metric, which scores stability, graspability, and clearance directly on sensor data. This metric enables model-free unified pick-and-place reasoning: by jointly scoring grasp and placement candidates, the system selects admissible grasps that lead to the most stable placements in cluttered real-world scenes.

lacks a generalized placeability metric that operates directly on sensor data (e.g., partial or noisy point clouds) and generalizes to arbitrary shapes.

To address these limitations, we introduce a novel *generalized placeability metric* that scores 6-DoF placement poses directly from an object’s point cloud without the need of any shape prior. Our metric fuses physical plausibility (object stability and clearance to other objects) with robot constraints (feasibility and collision avoidance with the gripper) and is computed online for an observed object. Using our metric, we derive various placement candidates with different orientations from raw geometry by extracting the object’s support surface for each and sampling contacts with collision-free and stable poses across the target region. This generalized placeability metric allows us to perform *model-free* unified pick-and-place reasoning.

Fig. 1 illustrates an example of our framework in action. We compute placement-conditioned graspability scores for each placement candidate’s frame, mapping predicted grasps to the object goal pose and checking for kinematic feasibility and collision avoidance. Representing the score formulation in vectorized form enables the efficient evaluation of large-scale sets of grasp-place pairs in real time, while remaining compatible with any grasp-prediction method. Our contribu-

tions can be summarized as follows:

- We introduce a generalized placeability metric, derived from task-inspired principles of stability, clearance, and graspability, that can be directly computed from noisy, partial point clouds without requiring CAD models.
- We propose an *object-centric* formulation for unified pick-and-place reasoning, that evaluates grasps in a common object frame and allows for direct reasoning over the shared feasible set.
- The physical validity of the stability term is demonstrated on unseen real objects and compared to a CAD-based baseline [6] on edge proximity and inclined surfaces, showing that our method accurately captures the loss of stability, whereas the baseline underestimates it. Furthermore the stability score is compared to a learning-based method [9] in terms of placement validity, demonstrating lower overall error and improved scalability with increasing object knowledge.

Furthermore, the utility of the proposed metric is shown in a model-free unified pick-and-place pipeline, showcasing its effectiveness for both grasping and placement.

The code of our complete pipeline will be made available upon publication.

II. RELATED WORK

A. Placeability Metrics

Various approaches have proposed metrics to quantify placeability [6], [7], [9], [10], [11], [12], [13], [14] where the focus is often to predict the stability of objects and identifying the most stable surface on which they can be placed on

Haustein *et al.* [6] proposed to search for collision-free and reachable object poses with stable placement, while optimizing a user-designed objective, such as maximizing or minimizing clearance to obstacles. However, in comparison to our proposed pick-and-place reasoning pipeline, their approach assumes full knowledge of both the object and environment models, restricts placements to planar surfaces, and does not consider grasp candidates during placement pose sampling, which may limit the number of feasible placements.

For unavailable ground truth object models, Noh *et al.* [9] addressed the problem of Unseen Object Placement (UOP) by introducing UOP-Net, a point cloud segmentation network. Given a single partial point cloud, UOP-Net predicts the most stable plane on which an object can be placed. While UOP-Net performs well in simulation and real-world trials, it assumes planar surfaces without placing close to edges, always outputs a single stable plane without a general placeability score, and excludes spherical or small objects.

Recently, Zhao *et al.* [13] proposed AnyPlace, which integrates vision-language models with diffusion-based pose prediction to infer context-driven placements from human input. AnyPlace focuses on receptacle-style scenarios such as insertion, stacking, and hanging, and achieves strong generalization by leveraging a large synthetic dataset together

with high-level VLM guidance. However, its formulation is specialized to language-conditioned receptacle placements and does not explicitly provide a general placeability metric or address robot feasibility constraints.

In contrast, our work introduces a generalized, model-free placeability metric that directly evaluates stability, clearance, and graspability from noisy point-cloud data. This enables online reasoning about feasible placements for previously unseen objects across diverse and constrained environments, while also supporting unified pick-and-place planning.

B. Pick-and-Place

Pick-and-place planning represents a core challenge in robotics and has been the focus of extensive research efforts [3], [4], [5], [8], [15], [16], [17], [18]. Recent work has increasingly explored joint pick-and-place planning, aiming to improve success rates and reduce computational overhead compared to sequential approaches. In more detail, Shanthi *et al.* [3] formulate pick-and-place as a constrained optimization problem, maximizing the joint probability of grasp and placement success. While this coupling leads to high placement success, it requires accurate success prediction models and can be sensitive to errors in these estimations. In comparison to the He *et al.* [5] propose an object-centric action space that jointly considers picking and placing actions for a given object. They employ neural radiance fields to encode scene geometry and generate affordance maps of feasible placements. While effective, the reliance on NeRF-based representations makes the approach computationally heavy and less suited for online use. Qin *et al.* [19] propose an energy-based model that jointly predicts grasp feasibility at the pick and place poses to directly infer shared grasps valid in both configurations, accelerating unified pick-and-place planning. The approach assumes a known, fixed environment, uses offline precomputed grasp candidates from a 3D mesh, and relies on large-scale training in simulation.

In contrast, our work adopts a model-free approach that evaluates a wide range of placement poses directly from point-cloud observations. By computing a general placeability metric online, we can efficiently select the best grasp-placement configuration and pass it to a motion planner. Unlike prior work, our method scales to many candidate placements without relying on heavy prediction networks, as the shared-grasp formulation provides a direct correspondence between pick and place poses, making it well suited for online deployment.

III. OUR APPROACH

We propose a generalized placeability metric, computed directly from observed point cloud data, which enables model-free unified pick-and-place reasoning by scoring 6-DoF placements in terms of stability, clearance, and their associated graspability. This enables the robot to reason about diverse placement poses in cluttered environments, ensuring robust and task-adaptive object positioning without relying on CAD models or predefined templates. In the following, we describe the design of our framework as

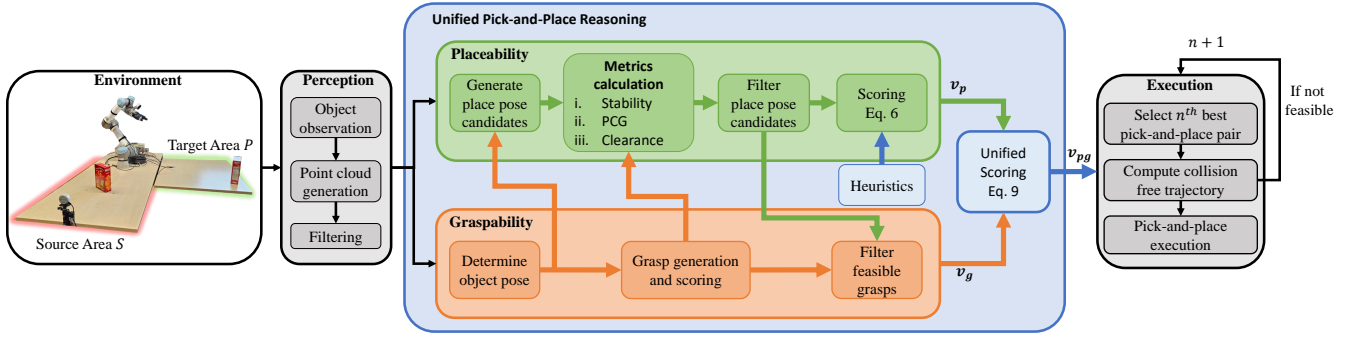


Fig. 2: Overview of our framework for model-free unified pick-and-place reasoning. The pipeline integrates perception, grasp generation, and placement evaluation into a single object-centric process. Point clouds are reconstructed from RGB-D observations to generate object and environment representations. Feasible grasps and candidate placements are then evaluated using our generalized placeability metric, which accounts for stability, placement-conditioned graspability (PCG), and clearance. A unified score combines these factors with heuristic constraints to select the best-scoring pick-and-place pair. Finally, motion planning and execution proceed by iterating through candidate pairs in descending score order until a feasible trajectory is found.

summarized in Fig. 2. First, we provide a formal problem definition and outline the perception pipeline for object and environment reconstruction. Then, we detail our novel placeability metric that scores each placement candidate by fusing placement-conditioned graspability (PCG), altitude-based clearance, and object stability. Finally, we detail our unified pick-and-place reasoning that vectorizes grasp-place evaluation and selects the execution that best realizes high-placeability outcomes.

A. Problem Formulation and Assumptions

We consider the following problem: Given an observed *source* region S , an observed *target* region P , and an observed object $o_i \in O$ with a priori unknown 6-DoF pose $m_o \in \text{SE}(3)$ inside S , the task is to compute physically stable, collision-free placement poses $m_p \in \text{SE}(3)$ inside P *without* any predefined placement template, i.e., orientation, position, or CAD model. The target area may exhibit clutter and tight spatial constraints, which in turn shape the robot's kinematic feasibility and collision margins. For reasoning, we assume that the target object can be sufficiently observed to obtain a partial object point cloud.

We reconstruct the workspace and the object online from RGB-D observations by fusing depth point clouds into a truncated signed distance function (TSDF) scene mesh \mathcal{M} [20]. In particular, from an initially unknown environment, we observe the scene from predefined view poses around an initial guess of the object's position and additional view poses that can sufficiently observe the key parts of the environment. Note that no a priori knowledge about the object's shape or orientation, as well as the pose of cluttered objects in P is assumed. After removal of outliers and further filtering on point clouds, meshes for individual objects and surrounding structures are extracted using marching cubes [21]. This representation supplies CAD-free, per-object geometry for placeability evaluation and a reliable collision mesh for the environment for motion feasibility checks.

B. Placeability Metric

To ensure robust object placement, we introduce an object-centric *placeability metric* that quantifies how suitable a

candidate placement pose m_p is for an object o_i using only its sensed visual geometry. The metric integrates three complementary scores: (i) A **point cloud based stability** measure that assigns higher scores to object placements whose projected center-of-mass hypotheses lie within the placing candidate's support polygon, ensuring robust equilibrium even under partial or noisy observations. (ii) A **placement-conditioned graspability** measure that evaluates whether high-quality grasps remain kinematically feasible and collision-free after being transformed into a candidate placement pose, thereby linking grasp success directly to the downstream placement outcome. (iii) An **altitude-based clearance** term that shapes the vertical clearance between the grasp and the object's lowest point, reducing the risk of unintended surface interactions during both grasping and placing. Optionally, these components can be modulated by task-specific heuristics, e.g., dense packing preferences.

1) **Object Stability:** To sample only stable 6D placement poses for an object o_i given its reconstructed point cloud, we assess whether the object will remain in static equilibrium once placed in the given pose. Given the support contact set at pose m_p , the support polygon $SP(o_i)$ is the 2D convex hull of contact points. We then draw center-of-mass (CoM) hypotheses from an ellipsoidal Gaussian $\mathcal{N}(\mu, \Sigma)$ fitted to the object point cloud \mathcal{P}_o , where the ellipsoidal mean μ is the average of the considered points. The size of the ellipsoid is computed by the maxima and minima of the object boundaries in the lateral and longitudinal axes while vertically only values with close proximity to μ are considered. Each sample is projected to the support plane to form a plausible CoM candidate $PC_n \in PC$.

The stability score is then calculated by a function based on the inlier fraction $p_{in} \in [0, 1]$ of PC samples whose vertical projection lie inside the polygon $SP(o_i)$. With $\sigma(x)$ being the logistic function, the stability score is given by:

$$f_{st}(p_{in}) = \frac{\sigma(k(p_{in} - c)) - \sigma(k(0.5 - c))}{\sigma(k(1.0 - c)) - \sigma(k(0.5 - c))} \quad (1)$$

where $k > 0$ controls the steepness of the transition and c is the center of the logistic. Note that we assume a locally

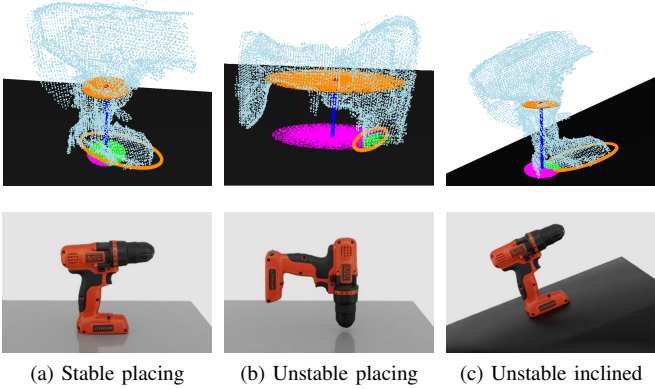


Fig. 3: Stability measure, illustrated on a noisy partial point cloud of a power drill with its front section missing. (a) **Stable**: most sampled points lie inside the support polygon, yielding a high score. (b) **Unstable**: most points fall outside, giving a near-zero score. (c) **Inclined**: despite full contact, the steep tilt projects points beyond the polygon, again producing a low score.

planar object support surface. For more complex object surfaces, the support model has to be adapted accordingly. Fig. 3 illustrates examples of the stability measure. In Fig. 3.a a stable placement is shown, where most sampled center points are projected inside the corresponding support polygon, resulting in a high stability score. In contrast, Fig. 3.b depicts an unstable pose in which most sampled points fall outside the SP, yielding a score close to zero. Finally, in Fig. 3.c, although the power drill rests on its entire SP, the steep inclination causes the projected points to extend beyond the polygon, producing a low stability value.

2) **Placement-Conditioned Graspability (PCG)**: To validate whether a candidate placement pose can actually be realized with the available grasps, we introduce placement-conditioned graspability, which evaluates if a grasp remains feasible once transformed into the placing pose frame. Let $\mathcal{G}(o_i) = \{g_0, \dots, g_k\}$ be the set of k candidate grasps for object o_i at the object’s observed pose m_o . Then, $T(m_p)$ denotes the rigid transform of a grasp g_k from its sampled grasp pose at m_o to a target pose m_p and the transformed grasp is defined as $g_k^p = T(m_p) \cdot g_k$. In practice, we first align the object into a local frame to sample grasps and then map those grasps back to the world frame. To compute the PCG, we score each candidate grasp at the placement pose m_p that remains reachable and collision-free as:

$$f_{\text{pcg}}(g_k^p) = q(g_k) \cdot \text{RM}(g_k^p) \cdot \text{coll}(g_k^p, \mathcal{M}) \quad (2)$$

where $q(\cdot)$ is the grasp score predicted by a grasp prediction strategy such as a neural network, $\text{RM}(\cdot) \in \{0, 1\}$ tests kinematic feasibility for the manipulator via a precomputed reachability map [22], and $\text{coll}(\cdot, \mathcal{M}) \in \{0, 1\}$ checks collision against the environment mesh \mathcal{M} of the target region.

3) **Altitude-Based Clearance**: To avoid collisions with the supporting surface, we weigh grasps by their vertical clearance relative to the object’s lowest sensed point. For a feasible grasp g_k^p , with height $z(g_k^p)$, at placement pose m_p ,

the clearance is:

$$\delta_z(m_p) = z(g_k^p) - \min(o_i) \quad (3)$$

We then assign a clearance weight using a logistic function:

$$f_{\text{alt}}(m_p | o_i) = w_{\min} + \frac{w_{\max} - w_{\min}}{1 + \exp(-k(\delta_z(m_p) - z_{\text{mid}}))}, \quad (4)$$

where $z_{\text{mid}} = \frac{1}{2}(z_{\text{start}} + z_{\text{end}})$ centers the transition, $k > 0$ controls its steepness, and $w_{\min}, w_{\max} \in [0, 1]$ set the range. Clearances below z_{start} are downweighted, while those above z_{end} saturate at w_{\max} .

4) **Task-Driven Placement Evaluation**: In addition to the individual components of our placeability metric, we define an optional, user-defined heuristic $f_H(\cdot)$ that assigns a score to each candidate placement pose or grasp to encode operational preferences (e.g. dense- or sparse-packing). To promote compact yet collision-free arrangements in the target region, we define the clearance of the object’s mesh o_p at pose m_p as the minimum distance to any other object in $o_i \in \mathcal{P}$:

$$d(m_p) = \min_{o_i \in \mathcal{P}} \text{dist}(o_p, o_i). \quad (5)$$

The dense-packing heuristic $f_{\text{H}_{\text{dp}}}(m_p) \in [0, 1]$ maps this clearance to a score. If the clearance is smaller than a collision margin, the candidate is rejected ($f_{\text{H}_{\text{dp}}}(m_p) = 0$). The score is maximal ($f_{\text{H}_{\text{dp}}}(m_p) = 1$), if the object is closer to other objects than threshold τ . For clearances $d(m_p) > \tau$, the score decays exponentially,

$$f_{\text{H}_{\text{dp}}}(m_p) = \exp(-k(d(m_p) - \tau)), \quad (6)$$

with $k > 0$ controlling the rate of decay. Thus, larger scores correspond to tighter packing while remaining safely non-colliding. Sparse-packing can be archived by inverting the distance calculation to $\tau - d(m_p)$

C. Unified Pick-and-Place Reasoning

After introducing our placeability metric, we now present our approach for model-free unified pick-and-place reasoning, which integrates grasp candidate prediction and selection, as well as placement evaluation into a single object-centric pipeline. This object-centric unified formulation enables the selection of grasps that not only succeed during picking but also remain effective for the subsequent placing task.

1) **Graspability Scoring**: For grasp planning on object point clouds, we utilize the Grasp Pose Detection (GPD) network [23]. For any object instance o_i , a set of candidate grasps G is computed, from which the top- k grasps $[k_0, \dots, k_n] \in G$ are retained based on their grasp scores $q(g_k)$ predicted by GPD. As GPD uses only rectangular cuboids for internal collision checking, we further validate candidate grasps for collisions using a simplified gripper model of our used manipulator, and only collision-free grasps are forwarded to the place planning stage. Note that we adopt GPD for its robustness and availability, but any grasp prediction method or network can be used to generate the necessary grasp in our pipeline, provided that the grasp can be represented by an SE(3) rigid body transformation.

2) **Placeability Scoring:** For placeability evaluation, we begin by sampling feasible object poses $m_p \in P$ of an object o_p within the mesh of target area P . Then, surface normals are computed at each sampled point, and random yaw rotations are applied to generate diverse orientations. The convex mesh of the object is evaluated at each sampled pose for collision with the environment, and only collision-free poses are retained.

To enable more versatile object placements, we evaluate a fixed set of discrete object orientations at each valid placement position. Specifically, we consider the initially observed orientation as well as 90° rotations around the $\pm x$ (pitch) and $\pm y$ (roll) axes, resulting in a total of six candidate orientations. Place pose validation of each possible orientation is performed by checking for collisions between the object's convex hull mesh and the environment mesh, while place-grasp feasibility is verified by testing collisions between the simplified gripper model and the environment.

Finally, we define possible place-grasps candidates g_k^p , which are scored by combining PCG, stability, and altitude metrics, along with an optional placement heuristic $f_H(\cdot)$, as described in Sec. III-B:

$$q(g_k^p) = f_{\text{pcg}}(g_k^p) \cdot f_{\text{st}}(m_p | o_p) \cdot f_{\text{alt}}(m_p | o_p) \cdot f_H(\cdot) \quad (7)$$

Furthermore, to enable comparison across candidates, we normalize the grasp and place-grasp scores:

$$v_g = \frac{q(g_k)}{\max(q(g_k))}, \quad v_p = \frac{q(g_k^p)}{\max(q(g_k^p))} \quad (8)$$

with v_g and v_p being represented as vectors sorted in descending order by value.

3) **Unified Object-Centric Reasoning:** Assuming k feasible grasps are available at the pick location, we evaluate their compatibility with each placement pose, i.e., we construct a binary collision matrix C_p to indicate whether grasp g_k remains collision-free when used at placement pose m_p

$$C_p(g_k, m_p) = \begin{cases} 0 & \text{if } g_k \text{ collides at } m_p \\ 1 & \text{otherwise} \end{cases} \quad (9)$$

To rank grasps according to both picking and placing feasibility, we define a unified grasp score that considers the original grasp quality, the quality of associated placements, and their collision status:

$$v_{gp} = \omega_g v_g \cdot \omega_p v_p \cdot C_p \quad (10)$$

where ω as weights.

This formulation inherently favors grasps that exhibit high intrinsic quality and are associated with stable, accessible placements. Finally, the grasp and placement combination with the highest score v_{gp} is selected for execution. This unified scoring encourages the selection of grasps that balance individual quality with environmental feasibility, ensuring consistent performance across both pick and place phases.

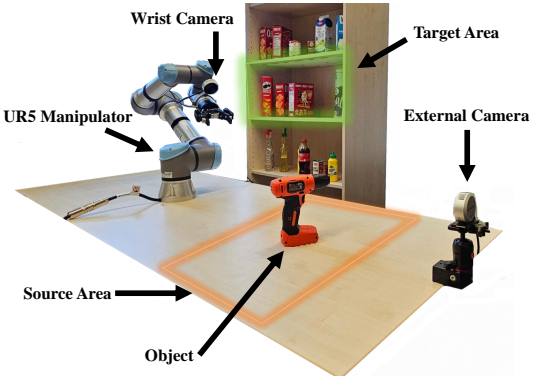


Fig. 4: Robotic setup used for the experiments.

IV. EXPERIMENTAL EVALUATION

We validate our proposed placeability metric for further potential use in a general pick-and-place pipeline using three experimental evaluations. First, we compare our method with UoP-Net [9] on partial point clouds of real-world unseen objects, evaluating both methods by measuring the potential positional offset resulting from the discrepancy between the predicted stable placement and the final object pose after physics simulation. Second, we test the physical fidelity of the stability term on non-ideal supports by measuring tipping thresholds near edges and critical inclination angles. Third, we assess system-level performance through success rate, runtime, and ablations isolating the stability component, and qualitative heuristic integration.

Experiments mostly use YCB objects [24] spanning diverse geometries and mass distributions. All experiments are conducted with a UR5e 6-DoF arm and Robotiq 2F-85 gripper. Perception relies on two Realsense L515 depth cameras (one wrist-mounted and one external camera), with the system running in ROS2 on an NVIDIA RTX 4080 Super GPU, an AMD Ryzen 9 7900X3D CPU, and 128 GB of RAM. Real-world partial point clouds are captured from multiple viewpoints, complemented by the external camera to extend the viewing range beyond the robot's workspace, as shown in Fig. 4.

A. Quantitative Evaluation on Object Stability

To assess the physical validity of our placeability metric, we focus on the object-stability term f_{st} . Although the overall metric also depends on placement-conditioned graspability and altitude clearance, these components are grasp-centric and do not directly encode the physical constraints of placing an object in an arbitrary orientation on a supporting surface. We conduct two main experiments. First, we compare our stability measure with the placing-surface prediction network UoP-Net [9] on previously real unseen objects. UoP-Net is the most closely related method because it operates on partial point clouds rather than CAD models and predicts a stable plane that approximates the object's surface on which it should be placed. Second, we evaluate our measure on non-continuous planar supports, i.e., table edges and inclined surfaces, compared to a CAD-based method [6].

Object	Method / View	Rot. [deg] ↓	Trans. [cm] ↓	L2 Full ↓
Power Drill	Ours (1-view)	3.843 ± 2.076	0.489 ± 0.498	0.095 ± 0.051
	UOP (1-view)	15.646 ± 6.015	2.006 ± 1.697	0.386 ± 0.145
	Ours (3-view)	5.939 ± 2.846	1.201 ± 0.823	0.147 ± 0.070
	UOP (3-view)	21.676 ± 17.813	1.868 ± 1.939	0.526 ± 0.424
Chips Can	Ours (1-view)	6.678 ± 2.074	3.559 ± 2.714	0.169 ± 0.153
	UOP (1-view)	27.558 ± 17.284	5.627 ± 3.653	0.671 ± 0.421
	Ours (3-view)	1.913 ± 1.486	0.195 ± 0.157	0.047 ± 0.036
	UOP (3-view)	9.746 ± 6.914	2.384 ± 2.048	0.243 ± 0.168
Mustard Bottle	Ours (1-view)	14.456 ± 22.038	1.685 ± 1.018	0.349 ± 0.527
	UOP (1-view)	9.916 ± 6.234	0.682 ± 0.385	0.244 ± 0.153
	Ours (3-view)	5.141 ± 2.212	0.728 ± 0.205	0.127 ± 0.054
	UOP (3-view)	23.935 ± 26.475	1.668 ± 1.603	0.572 ± 0.618
Cracker Box	Ours (1-view)	7.468 ± 5.442	5.532 ± 6.375	0.197 ± 0.140
	UOP (1-view)	5.832 ± 4.521	3.135 ± 3.309	0.148 ± 0.115
	Ours (3-view)	3.537 ± 1.165	0.930 ± 0.152	0.088 ± 0.029
	UOP (3-view)	2.210 ± 1.720	0.433 ± 0.474	0.055 ± 0.043

TABLE I: Evaluation of object stability from partial point clouds with single or fused viewpoints. We compare our method to UOP-Net [9] on three YCB objects, using pose accuracy as a proxy for stability. Placement poses are computed from real point cloud observations and simulated, where instability manifests as larger pose deviations (rotation, translation, and L2 error). The results indicate robustness of our method under partial and noisy observations and adaptability to new information.

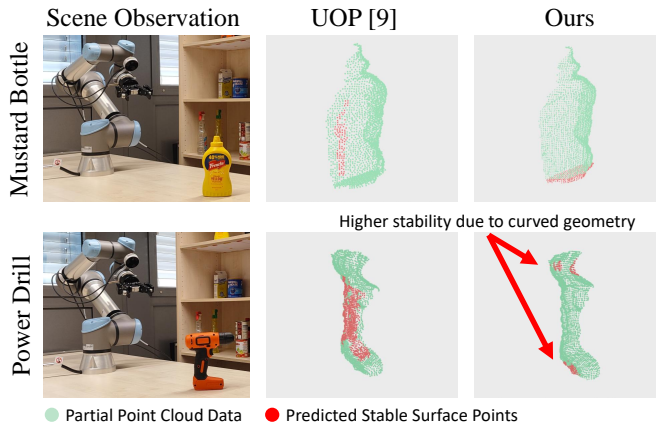


Fig. 5: Qualitative comparison of predicted stable surfaces between our method and UOP [9]. Our approach consistently identifies a physically stable placement even from noisy partial point cloud data, whereas UOP often predicts unstable placements. Both methods place the mustard bottle on stable contact points. In the case of the power drill, it cannot be placed on the surface predicted by UOP due to its curved geometry, whereas our method correctly identifies the peak contact points that allow for a stable placement.

1) **General Object Stability Prediction:** We compare our physics-based stability metric against the neural network UoP-Net [9], using the authors' publicly available codebase and pretrained weights, and recorded real-world partial point clouds of four YCB objects (power drill, cracker box, mustard bottle, and chips can). Since UoP-Net demonstrates strong results from single viewpoints in its original work, we generated four distinct partial point clouds per object, each corresponding to one of four possible viewpoints. This setup resembles realistic partial observations and achieves an average mesh coverage of $35.1\% \pm 6.5\%$, ensuring comparable input quality across methods.

For each object, we obtain the surface that the network predicts as most stable and, in parallel, compute the corresponding candidate surface using our own method, after which both sets of candidates were tested for stability in simulation. In each trial, we initialized the object such that

the candidate support surface was in contact with a planar table and then simulated whether the object would remain at rest. Stability was quantified using the positional offset metrics (rotation, translation, and L2 norm) proposed in [9], computed between the object's pose before placement and after simulation. We chose to evaluate stability in simulation because single viewpoint inputs can occasionally lead to support surface predictions that penetrate the object volume (see Fig. 5), a behavior sensitive to partial point-cloud quality and noise assumptions that differ from those in the original evaluation and are unsafe to execute in the real world. The results in Tab. I show that our method outperforms UoP-Net on objects of complex geometry, while performance remains comparable and occasionally favors UoP-Net for simpler shapes. We showcase two qualitative examples of predicted surfaces in Fig. 5, where our method results in a better stable surface prediction in case of the power drill, due to its curved geometry. Overall, these results indicate that our stability prediction is robust to partial and noisy observations and benefits from increased coverage using multiple viewpoint.

2) **Tipping Point Prediction:** Beyond horizontal surfaces, it is crucial to determine whether an object remains stable on arbitrary supporting surfaces. However, UoP-Net is limited to predicting horizontal support surfaces for planar placement and does not provide this functionality. We therefore evaluate our stability metric in two challenging scenarios outside standard planar placement, i.e., (i) edge proximity, where we estimate the tipping threshold when an object is positioned near a boundary such as the edge of a table or shelf, and (ii) surface inclination, where we assess stability on tilted supports that can arise from stacked objects or uneven furniture. A robust stability metric should indicate that, once a critical offset is exceeded, the object will tip and no static equilibrium exists. Because both the critical edge offset and the critical tilt angle depend strongly on object geometry and mass distribution, the metric should encode these dependencies reliably.

We evaluate the metric on three YCB objects (power drill, mustard bottle, and cracker box). Furthermore, for the power drill, we consider two orientations, since its displaced center of mass causes the object to tip earlier on one side (backwards) than on the other. The CAD model's center of mass (COM) [6] is used as a baseline for the tipping point. For edge proximity, we obtained ground-truth tipping thresholds on real-world objects by slowly pushing each object toward the boundary until static equilibrium was lost, and we report the threshold as a percentage of the object's support footprint. The results in Fig. 6 show that our stability curves exhibit a sharp transition near the measured real-world tipping threshold (red dashed line) across all objects and orientations. The method correctly predicts that the power drill tips earlier in the backwards orientation than in the forward orientation. As viewpoint count increases (and thus surface coverage improves), the transition becomes steeper and converges to the 100% coverage curve, indicating robustness to partial/noisy observations. In contrast, the CAD's COM baseline (gray dotted) can deviate around the threshold

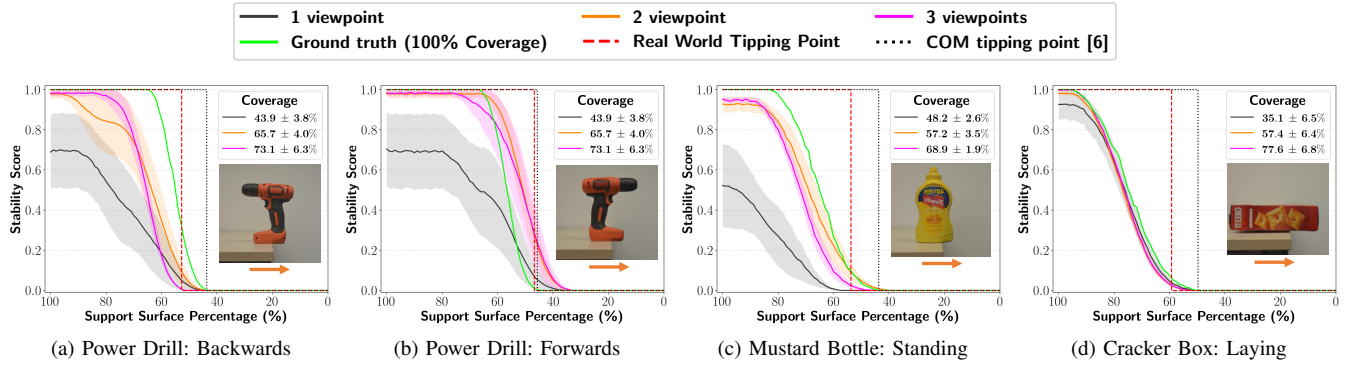
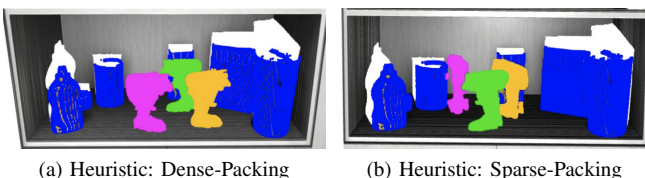
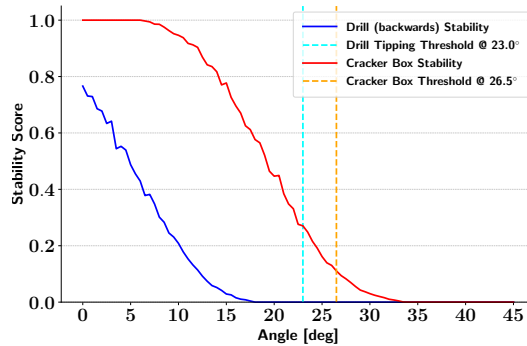


Fig. 6: Table-edge proximity tipping analysis for three YCB objects—power drill (two orientations), mustard bottle (upright), and cracker box (lying flat). The plots show our stability score against the fraction of the object’s support footprint that remains on the table as the object is translated toward the edge. Colored curves correspond to fused point clouds from 1–3 viewpoints, with the inset reporting the average visible-surface coverage in each case. The red dashed vertical line marks the real-world tipping threshold, obtained by gradually pushing the object until static equilibrium was lost. The gray dotted line indicates the CAD-based COM prediction [6], while the “100% coverage” curve approximates the ideal case with complete geometry from the CAD model under our method. Across objects and orientations, our metric closely tracks the critical offset and converges toward the ground-truth threshold as coverage increases.



because it ignores contact geometry and partial support. For surface inclination, we use simulation to ensure repeatability, gradually increasing the tilt until the object topples. As shown in Fig. 7, the stability score decreases monotonically with tilt and collapses near the simulated tipping angle, aligning closely with ground truth (e.g., $\approx 23^\circ$ for the power drill, $\approx 26.5^\circ$ for the cracker box). These results confirm that the proposed metric reliably encodes geometry- and mass-dependent stability on non-planar supports.

B. Qualitative Validation of Task-Driven Constraints

To further validate the physical realism of our placeability metric, we present qualitative results under task-driven constraints. As described in Sec. III-B.4, our reasoning pipeline can incorporate heuristics that impose task-driven constraints beyond pure feasibility checking. Fig. 8 illustrates a shelf scenario for two such heuristics, with green denoting the highest placeability score and magenta the lowest. In Fig. 8a, a dense-packing heuristic favors small inter-object distances, i.e., our planner assigns the top score to a location near other items at the shelf’s end, while more distant placements receive lower scores. Conversely, Fig. 8b applies a sparse-packing heuristic that favors larger separations, shifting the highest scores to positions farther from existing objects. Together, these results demonstrate that our pipeline can be easily adapted to enforce task-driven constraints. The computation of this heuristic required 3.51 ± 3.18 seconds on average over 100 runs.

C. Runtime Analysis

To assess the online performance of our full pick-and-place reasoning pipeline, we measured the total reasoning time for object placement in clutter across five objects (chips can, cracker box, power drill, milk, mustard bottle). Each object was tested in 10 trials within a shelf environment containing 7–10 other YCB objects and with different numbers of grasp candidates (100, 250, 500). We exclude the computation time of GPD, since our pipeline is agnostic to the specific grasp generation method used.

As shown in Fig. 9, the total runtime remains largely stable as the number of candidates increases. Object geometry causes the variation: for a maximum of 500 sampled grasps, the mustard bottle takes the longest—consistent with its irregular, non-planar surfaces—whereas the cracker box is fastest due to its simple cuboid shape and straightforward placements. Tab. II breaks down the timing for the YCB drill. The unified reasoning module is essentially negligible (0.0005 s), while environment reconstruction is the primary bottleneck (5.9423 s), followed by placability evalua-

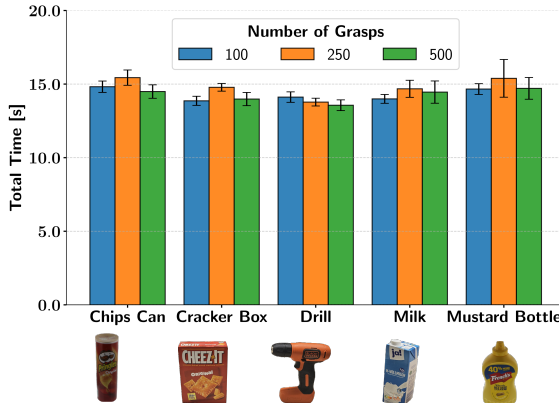


Fig. 9: Detailed runtime analysis of our pick-and-place reasoning pipeline across five objects of varying shape complexity, averaged over 10 runs in shelf environments containing seven to ten other objects. The results show that our pipeline maintains stable runtimes even as the number of candidate grasps increases.

tion (4.0053 s) and collision checking (3.6137 s). Importantly, while placeability evaluation introduces additional cost, it is central to our approach, as it helps achieve more stable object placement while providing functionality of the tipping point prediction absent in existing methods. In contrast, our unified grasp-place reasoning adds virtually no overhead.

D. Unified Pick-and-Place Reasoning on Real Hardware

While the focus of this work lies on the unified reasoning, we additionally provide a qualitative demonstration to illustrate its practical applicability. A real-world pick-and-place sequence executed by the UR5 in a shelf environment is shown in Fig. 10. Starting from initial observations of the object in the source area S and the target area P , the system reconstructs partial point clouds of both regions. Based on these observations, it samples a diverse set of candidate placement poses and scores them according to their stability. For each pose, it uses the two further metric components (Sec. III-B) to evaluate feasibility with respect to the grasp candidates predicted at the source by the grasp network. By considering different grasp–placement combinations for the same object, our unified reasoning framework selects the most stable and executable pair and successfully performs the task on the physical robot. Accordingly, the choice between a top or side grasp, and whether the object is placed in the same orientation or reoriented, directly depends on the available grasp candidates. Fig. 10 demonstrates this dependency by showing two contrasting situations. We executed our pipeline two times, in the top right sequence, the system is provided a top-down grasp, while in the bottom sequence a side grasp is used. Note that using the top-down grasp makes placement in the same orientation infeasible due to arm–shelf collisions. Consequently, the system deliberately reorients the object to achieve a collision-free and stable placement. If a side grasp was available that allowed direct placement without reorientation, the system would prefer that option instead and place the object in the same orientation as no collisions with the shelf would occur as shown in the bottom right sequence.

Component	Mean [s]	Std [s]
Reasoning	0.0005	0.0002
Placability	4.0053	0.0857
Collision	3.6137	0.0539
Reconstruction	5.9423	0.3355

TABLE II: Detailed runtime analysis of individual components for the YCB power drill (500 grasps). Reported are mean runtimes with standard deviations. The majority of computation time is spent on environment reconstruction for collision checking, whereas our unified reasoning module computes extremely efficiently, requiring only negligible time to select the optimal grasp–place pair

V. CONCLUSION

In this work, we presented a generalized placeability metric that enables model-free unified pick-and-place reasoning directly from noisy partial point clouds and finding different feasible object poses. By jointly evaluating stability, placement-conditioned graspability, and clearance, our metric provides a physically grounded and efficient basis for online reasoning in cluttered environments.

Experiments on YCB objects showed that our method predicts stability beyond planar assumptions, capturing edge and inclination tipping thresholds. Compared to UOP-Net [9] and CAD-based baselines, it achieved higher accuracy with lower rotational and translational errors, while adding negligible runtime. We also demonstrated task-driven heuristics for dense and sparse packing, and validated the full pipeline on a UR5 robot, showing coherent grasp–place sequences in cluttered shelves. These results confirm that our framework is both physically grounded and directly applicable to real-world manipulation.

REFERENCES

- [1] T. Li, Y. Yan, C. Yu, J. An, Y. Wang, and G. Chen, “A comprehensive review of robot intelligent grasping based on tactile perception,” *Robotics and Computer-Integrated Manufacturing*, vol. 90, 2024.
- [2] H. Zhang, J. Tang, S. Sun, and X. Lan, “Robotic grasping from classical to modern: A survey,” *arXiv preprint arXiv:2202.03631*, 2022.
- [3] M. D. Shanthi and T. Hermans, “Pick and place planning is better than pick planning then place planning,” *IEEE Robotics and Automation Letters (RA-L)*, vol. 9, no. 3, 2024.
- [4] J. Park, D. Jin, and K. Lee, “Placement aware grasp planning for efficient sequential manipulation,” in *Frontiers in Artificial Intelligence and Applications (FAIA)*, vol. 392, IOS Press, 2024.
- [5] Z. He, N. Chavan-Dafle, J. Huh, S. Song, and V. Isler, “Pick2place: Task-aware 6dof grasp estimation via object-centric perspective affordance,” in *Proc. of the IEEE Intl. Conf. on Robotics & Automation (ICRA)*, 2023.
- [6] J. A. Haustein, K. Hang, J. Stork, and D. Kragic, “Object placement planning and optimization for robot manipulators,” in *Proc. of the IEEE/RSJ Intl. Conf. on Intelligent Robots and Systems (IROS)*, 2019.
- [7] K. Harada, T. Tsuji, K. Nagata, N. Yamanobe, and H. Onda, “Validating an object placement planner for robotic pick-and-place tasks,” *Robotics and Autonomous Systems*, vol. 62, no. 10, 2014.
- [8] B. H. Leebron, K. Ren, Y. Chen, and K. Hang, “B4p: Simultaneous grasp and motion planning for object placement via parallelized bidirectional forests and path repair,” *arXiv preprint arXiv:2504.04598*, 2025.
- [9] S. Noh, R. Kang, T. Kim, S. Back, S. Bak, and K. Lee, “Learning to place unseen objects stably using a large-scale simulation,” *IEEE Robotics and Automation Letters (RA-L)*, 2024.
- [10] A. Holladay, J. Barry, L. P. Kaelbling, and T. Lozano-Pérez, “Object placement as inverse motion planning,” in *Proc. of the IEEE Intl. Conf. on Robotics & Automation (ICRA)*, 2013.

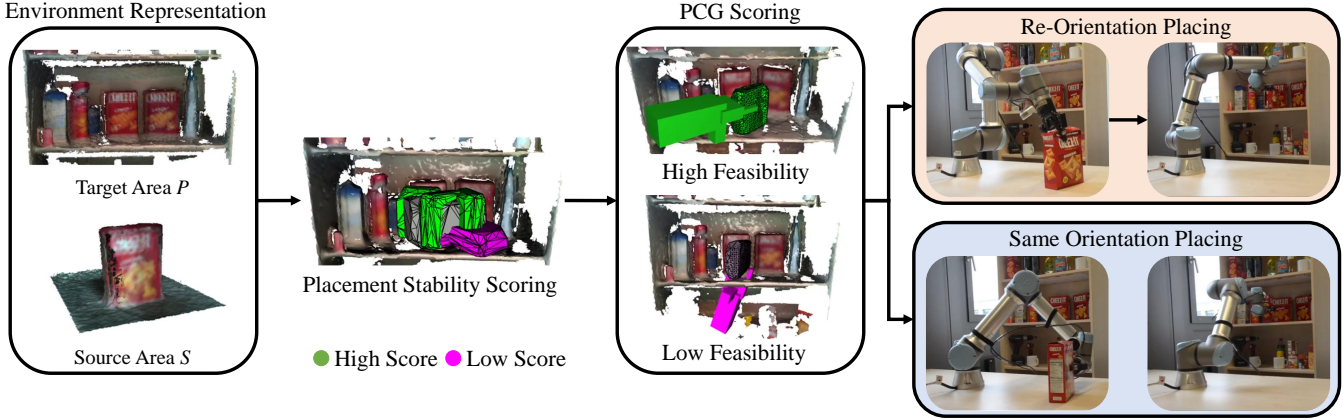


Fig. 10: From initial observations of the object in the source area S and the target area P , we reconstruct partial point clouds of both regions. Our method then samples a diverse set of candidate placement poses and scores them based on their stability. For each placement candidate, we evaluate its feasibility with respect to multiple predicted grasp poses. By considering different grasps for the same placement pose, the system is able to select the optimal grasp–placement combination. The figure also illustrates how the availability of predicted grasps affects the final strategy. We executed our pipeline two times, in the top right sequence, a top-down grasp is provided to the planner, whereas in the bottom right sequence, a side grasp is used by the planner, leading to different placement executions.

- [11] J. Lee, S. Park, J. Park, K. Lee, and S. Choi, “Spots: Stable placement of objects with reasoning in semi-autonomous teleoperation systems,” in *Proc. of the IEEE Intl. Conf. on Robotics & Automation (ICRA)*, 2024.
- [12] Y. Qin, J. Xu, R. Wang, and X. Chen, “Think before placement: Common sense enhanced transformer for object placement,” in *Proc. of the Europ. Conf. on Computer Vision (ECCV)*, Springer, 2024.
- [13] Y. Zhao, M. Bogdanovic, C. Luo, S. Tohme, K. Darvish, A. Aspuru-Guzik, F. Shkurti, and A. Garg, “Anyplace: Learning generalized object placement for robot manipulation,” *arXiv preprint arXiv:2502.04531*, 2025.
- [14] C. Paxton, C. Xie, T. Hermans, and D. Fox, “Predicting stable configurations for semantic placement of novel objects,” in *Proc. of Conf. on Robot Learning (CoRL)*, PMLR, 2022.
- [15] A. Lobbezoo, Y. Qian, and H.-J. Kwon, “Reinforcement learning for pick and place operations in robotics: A survey,” *Robotics*, vol. 10, no. 3, 2021.
- [16] M. Suomalainen, Y. Karayannidis, and V. Kyrki, “A survey of robot manipulation in contact,” *Journal on Robotics and Autonomous Systems (RAS)*, vol. 156, 2022.
- [17] M. Pantano, T. Eiband, and D. Lee, “Capability-based frameworks for industrial robot skills: A survey,” in *Proc. of IEEE Intl. Conf. on Automation Science and Engineering (CASE)*, IEEE, 2022.
- [18] E. Maranci, S. D’Avella, P. Tripicchio, and C. A. Avizzano, “Enabling grasp synthesis approaches to task-oriented grasping considering the end-state comfort and confidence effects,” *IEEE Robotics and Automation Letters (RA-L)*, vol. 9, no. 6, 2024.
- [19] L. Qin, W. Wan, J. Takahashi, R. Negishi, M. Matsushita, and K. Harada, “Learning from planned data to improve robotic pick-and-place planning efficiency,” *arXiv preprint arXiv:2506.15920*, 2025.
- [20] J. M. C. Marques, A. J. Zhai, S. Wang, and K. Hauser, “On the overconfidence problem in semantic 3d mapping,” in *Proc. of the IEEE Intl. Conf. on Robotics & Automation (ICRA)*, 2024.
- [21] W. E. Lorensen and H. E. Cline, “Marching cubes: A high resolution 3d surface construction algorithm,” in *Seminal graphics: pioneering efforts that shaped the field*, 1998.
- [22] Zacharias, Borst, and Hirzinger, “Capturing robot workspace structure: Representing robot capabilities,” in *Proc. of the IEEE/RSJ Intl. Conf. on Intelligent Robots and Systems (IROS)*, 2007.
- [23] A. Ten Pas, M. Gualtieri, K. Saenko, and R. Platt, “Grasp pose detection in point clouds,” *Intl. Journal of Robotics Research (IJRR)*, vol. 36, no. 13–14, 2017.
- [24] B. Calli, A. Singh, A. Walsman, S. Srinivasa, P. Abbeel, and A. M. Dollar, “The ycb object and model set: Towards common benchmarks for manipulation research,” in *Proc. of the Intl. Conf. on Advanced Robotics (ICAR)*, IEEE, 2015.